Diabetic retinopathy is associated with bone marrow neuropathy and a depressed peripheral clock

Julia V. Busik,[1] Maria Tikhonenko,[1] Ashay Bhatwadekar,[3] Madalina Opreanu,[1,2] Nafissa Yakubova,[1] Sergio Caballero,[3] Danny Player,[4] Takahiko Nakagawa,[4] Aqeela Afzal,[3] Jennifer Kielczewski,[3] Andrew Sochacki,[1] Stephanie Hasty,[1] Sergio Li Calzi,[3] Sungjin Kim,[2] Shane K. Duclas,[6] Mark S. Segal,[4] Dennis L. Guberski,[6] Walter J. Esselman,[2] Michael E. Boulton,[5] and Maria B. Grant[3]

[1]Department of Physiology and [2]Department of Microbiology and Molecular Genetics, Michigan State University, East Lansing, MI 48824
[3]Department of Pharmacology and Therapeutics, [4]Department of Internal Medicine, and [5]Department of Anatomy and Cell Biology, University of Florida, Gainesville, FL 32611
[6]Biomedical Research Models, Inc., Worcester, MA 01606

The present epidemic of diabetes is resulting in a worldwide increase in cardiovascular and microvascular complications including retinopathy. Current thinking has focused on local influences in the retina as being responsible for development of this diabetic complication. However, the contribution of circulating cells in maintenance, repair, and dysfunction of the vasculature is now becoming appreciated. Diabetic individuals have fewer endothelial progenitor cells (EPCs) in their circulation and these cells have diminished migratory potential, which contributes to their decreased reparative capacity. Using a rat model of type 2 diabetes, we show that the decrease in EPC release from diabetic bone marrow is caused by bone marrow neuropathy and that these changes precede the development of diabetic retinopathy. In rats that had diabetes for 4 mo, we observed a dramatic reduction in the number of nerve terminal endings in the bone marrow. Denervation was accompanied by increased numbers of EPCs within the bone marrow but decreased numbers in circulation. Furthermore, denervation was accompanied by a loss of circadian release of EPCs and a marked reduction in clock gene expression in the retina and in EPCs themselves. This reduction in the circadian peak of EPC release led to diminished reparative capacity, resulting in the development of the hallmark feature of diabetic retinopathy, acellular retinal capillaries. Thus, for the first time, diabetic retinopathy is related to neuropathy of the bone marrow. This novel finding shows that bone marrow denervation represents a new therapeutic target for treatment of diabetic vascular complications.

CORRESPONDENCE
Maria B. Grant:
grantma@ufl.edu
OR
Julia V. Busik:
busik@msu.edu

Abbreviations used: EPC, endothelial progenitor cell; HSC, hematopoietic stem cell; mRNA, messenger RNA; NE, norepinephrine; NF200, neurofilament 200; SCN, suprachiasmatic nucleus; TH, tyrosine hydroxylase; VEGF, vascular endothelial growth factor; ZT, Zeitgeber time.

Endothelial dysfunction is central to the development of diabetic macro- and microvascular complications, and it is these complications that contribute to the major morbidity and mortality for diabetic patients. Bone marrow–derived progenitor cells play a critical role in endothelial repair (Asahara et al., 1997; Grant et al., 2002). Endothelial progenitor cells (EPCs) arising from the bone marrow circulate in the bloodstream and home to areas of injury to orchestrate vascular repair (Grant et al., 2002). Recently, it was determined that the release of all bone marrow–derived cells occurs in a distinct circadian pattern (Méndez-Ferrer et al., 2008). The suprachiasmatic nucleus (SCN) in the central nervous system initiates this and other circadian rhythms as well as synchronizing peripheral clocks in organs and tissues. Circadian rhythms occur via

J.V. Busik, M. Tikhonenko, and A. Bhatwadekar contributed equally to this paper.

The Rockefeller University Press $30.00
J. Exp. Med. Vol. 206 No. 13 2897-2906
www.jem.org/cgi/doi/10.1084/jem.20090889

The Journal of Experimental Medicine

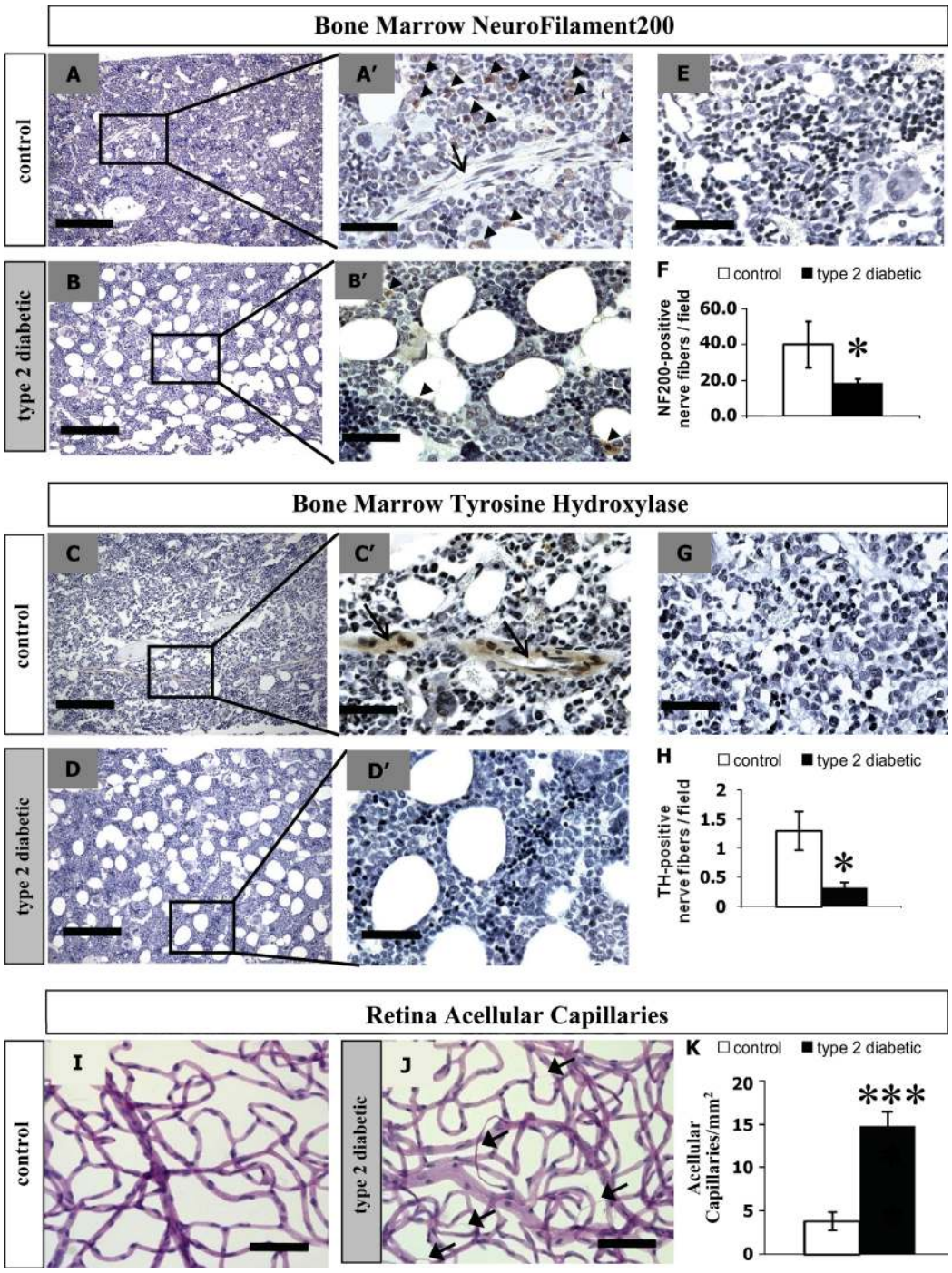

Figure 1. Dramatic decrease in humerus bone marrow innervation in diabetic rats is associated with an increase in retinal acellular capillaries. (A and B) NF200-positive nerve processes (arrowheads) are visible in bone marrow of control rats (A and A′) but significantly decreased in diabetic rats (B and B′). (C and D) TH-positive nerve processes running along blood vessels (arrows) were present in the bone marrow of controls (C and C′) but very rare in diabetic animals (D and D′). (E and G) No staining was found in negative controls treated only with secondary antibody. Bars: (A–D) 20 µM; (A′–D′, E, and G) 5 µM. (F and H) Quantification of the NF200 and TH data are shown in F and H, respectively. Diaphysis of the humerus bone from control ($n = 4$) and diabetic ($n = 3$) animals were assessed. At least 10 fields per humerus were analyzed on duplicate slides from each bone by three independent individuals. *, $P < 0.05$. The experiment was repeated on two independent sets of animals. (I and J) Retinal vasculature from control (I) and diabetic (J) animals was prepared using trypsin digestion and stained with hematoxylin and periodic acid–Schiff. Dramatically increased number of acellular capillaries (black arrows) was observed in retinal vasculature isolated from diabetic animals (I) compared with control (J). (K) Quantification of I and J. Bars, 10 µM. The data represent mean ± SD of three independent sets of animals, with nine control and nine diabetic animals total. At least eight fields per retina were counted in duplicates by two independent investigators. ***, $P < 0.001$.

autoregulatory transcriptional-translational feedback loops consisting of a defined set of clock genes. Pathological clock gene expression leads to diverse pathophysiological disorders including metabolic syndrome, obesity, premature aging, and abnormal sleep cycle (Weber, 2009). The physiological relevance of a disturbed circadian rhythm in diabetes is indicated by the observation that myocardial dysfunction, acute coronary syndrome, sudden cardiac death, and ischemic stroke occur with peak incidence in nondiabetics in the early morning, yet in diabetic patients the peak is at night (Weston and Gill, 1999; Ruiter et al., 2006; Ikeda et al., 2007; Peschke, 2008; Thomas et al., 2008). Interestingly, *db/db* mice, a model of type 2 diabetes, have disrupted circadian variation of blood pressure, heart rate, and locomotor activity, which are each associated with dampened oscillations of peripheral clock genes (Su et al., 2008).

Mobilization of EPC from the bone marrow occurs after activation of peripheral noradrenergic neurons and release of norepinephrine (NE), which suppresses osteoblast activity (Serre et al., 1999; Méndez-Ferrer et al., 2008). This results in a local decrease in SDF-1 (stromal-derived factor 1) and subsequent EPC mobilization from the bone marrow (Katayama et al., 2006). Advanced diabetes is associated with neuropathy (Said, 2007). We reasoned that diabetes-associated peripheral and/or autonomic neuropathy would reduce bone marrow innervation and thus reduce hematopoietic stem cell (HSC)/EPC release from the bone marrow. Decrease in circulating EPCs would reduce repair of injured retinal vessels in diabetics and lead to development of acellular capillaries, the hallmark feature of irreversible diabetic retinopathy.

RESULTS AND DISCUSSION

BBZDR/Wor rats with 4 mo of diabetes were used and compared with their age-matched nondiabetic BBDR littermates. The BBZDR/Wor rat was specifically developed as a model of type 2 diabetes that develops diabetic complications. Male obese BBZDR/Wor rats spontaneously develop diabetes that mimics human type 2 diabetes, and this typically occurs at 74 d of age. They demonstrate hyperglycemia and dyslipidemia, which are typical of type 2 diabetes, with increased levels of cholesterol, triglycerides, and nonesterified fatty acids (Tirabassi et al., 2004). The BBZDR/Wor rat develops retinopathy, neuropathy, nephropathy, and macrovascular complications typical of human type 2 diabetes and is emerging as the most applicable model of type 2 diabetic complications (Tirabassi et al., 2004). BBZDR/Wor animals demonstrate increased vascular endothelial growth factor (VEGF) production and increased VEGF receptor expression (Ellis et al., 2000), as well as increased NADPH oxidase activity (Ellis et al., 1998) and hydrogen peroxide production (Ellis et al., 2000) in the retinal vasculature as early as 2 wk after diabetes onset. BBZDR/Wor rats also progress to early preproliferative diabetic retinopathy with the development of acellular capillaries, pericyte ghosts, and capillary basement membrane thickening after 4 mo of diabetes (Tirabassi et al., 2004).

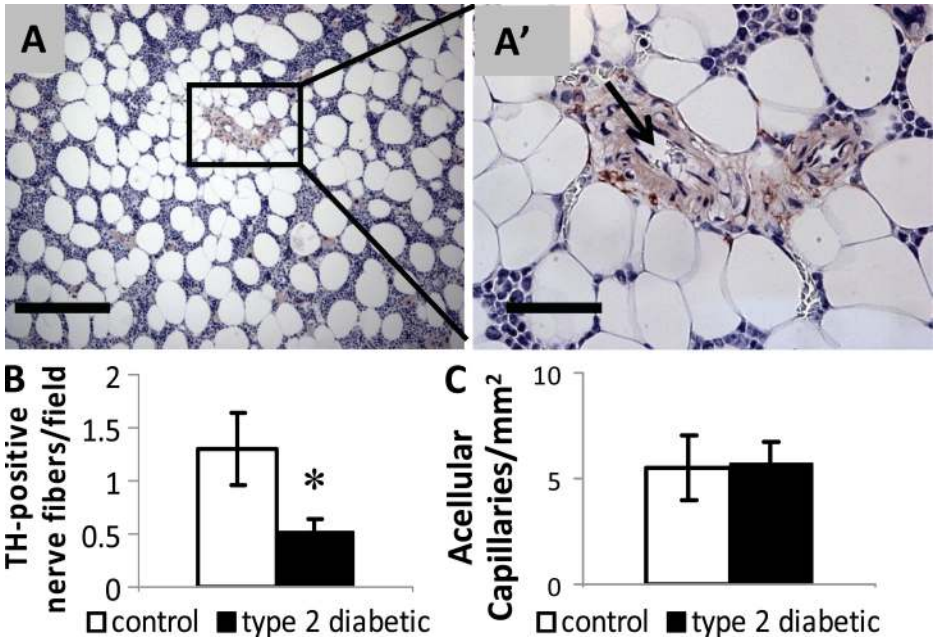

Figure 2. Denervation of the bone marrow precedes acellular capillaries formation in diabetic rats after 2 mo of diabetes. (A and B) TH-positive nerve processes running along blood vessel (arrow) were present in diabetic bone marrow at 2 mo of diabetes (A and A′) but were significantly decreased compared with controls (B). At least 10 fields were analyzed on duplicate slides from each bone by three independent individuals. Bars: (A) 20 µm; (A′) 5 µm. *, $P < 0.05$. The experiment was repeated on two independent sets of animals. Data are presented as the mean ± SD of four control and three diabetic (A and B) rats. (C) On the contrary, the number of acellular capillaries was not changed. Data in C are presented as the mean of two independent sets of animals, with six control and six diabetic rats total. At least eight fields per retina were counted in duplicates by two independent investigators. *, $P < 0.05$.

To explore the role of the sympathetic nervous system in the release of EPCs in diabetes, we first undertook an analysis of bone marrow histology and determined 24-h circulating NE levels. Histological examination of the bone marrow in rats with 4 mo of diabetes revealed a marked reduction in the number of nerve endings as determined by neurofilament 200 (NF200) staining and increased bone marrow lipid deposition compared with age-matched controls (Fig. 1, A–F). Tyrosine hydroxylase (TH) staining showed positive nerve processes running along blood vessels in the bone marrow of controls (Fig. 1, C and C′) but was very rarely found in diabetic animals (Fig. 1, D and D′), demonstrating a defect in sympathetic innervation. As shown in Fig. 1, 4 mo of diabetes resulted in the appearance of increased numbers of acellular capillaries within the retina (Fig. 1, J and K) compared with age-matched controls (Fig. 1, I and K). We observed that denervation of the bone marrow preceded the development of this retinal pathology because at 2 mo of diabetes, the rats did not have any retinal histopathological changes (Fig. 2 C) but already showed early signs of denervation (Fig. 2, A and B).

In these studies, we characterized the progenitor population based on surface expression of thy-1 and CD133 (Peichev et al., 2000), endothelial nitric oxide synthase expression (Loomans et al., 2006), and the ability of these cells to incorporate into capillary tubes in vitro (Schatteman et al., 2007; Fig. 3). To determine whether denervation of bone marrow affected circadian EPC release in diabetes, peripheral blood EPCs were enumerated by flow cytometry analysis every 2 h in diabetic rats and compared with age-matched controls. Control rats showed a dramatic peak of circulating EPCs between ZT (Zeitgeber time) 1 and ZT-5 (Fig. 4 A). In contrast, diabetic animals exhibited a marked reduction in the amplitude and a broader peak in the number of circulating EPCs between ZT-21 and ZT-7. Moreover, the controls

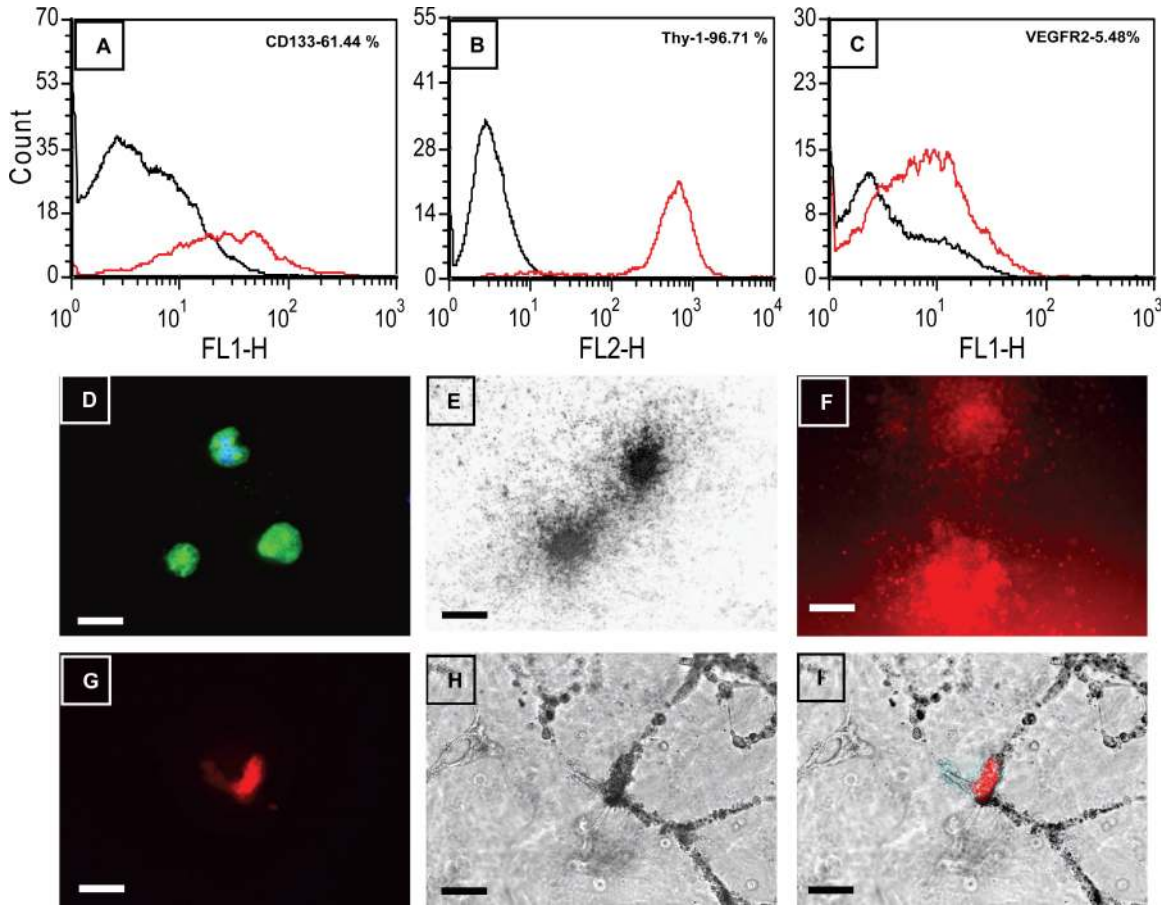

Figure 3. Rat thy-1⁺ cell characterization. Thy-1⁺ cells isolated from rat bone marrow were analyzed by FACS for progenitor marker expression. (A–C) Isolated cells express CD133 (A), Thy-1 (B), and VEGFR-2 (C). The red line represents the samples incubated with respective antibody. The black line in the representative histogram plot corresponds to the samples incubated with the appropriate isotope control antibodies. (D) Thy-1⁺ progenitors express endothelial nitric oxide synthase (green) as detected by immunofluorescence with nuclei stained with DAPI (blue). Bar, 10 µM. (E and F) Cells in culture form colonies (E) and incorporate DiI-acLDL (red; F). Thy-1⁺ cells incorporate into capillary tubes with human retinal endothelial cells. (G) Fluorescently labeled Thy-1 cells (red) incorporating into HRECs. (H) Phase contrast image of same region as in G. (I) Merged phase contrast and fluorescence images of Thy-1⁺ cells (red) participating in tube formation. Bar, 100 µM. Flow cytometry data are represented as percentage of cells expressing respective marker for rats ($n = 3$). Images are representative of $n = 4$ of individual experiments.

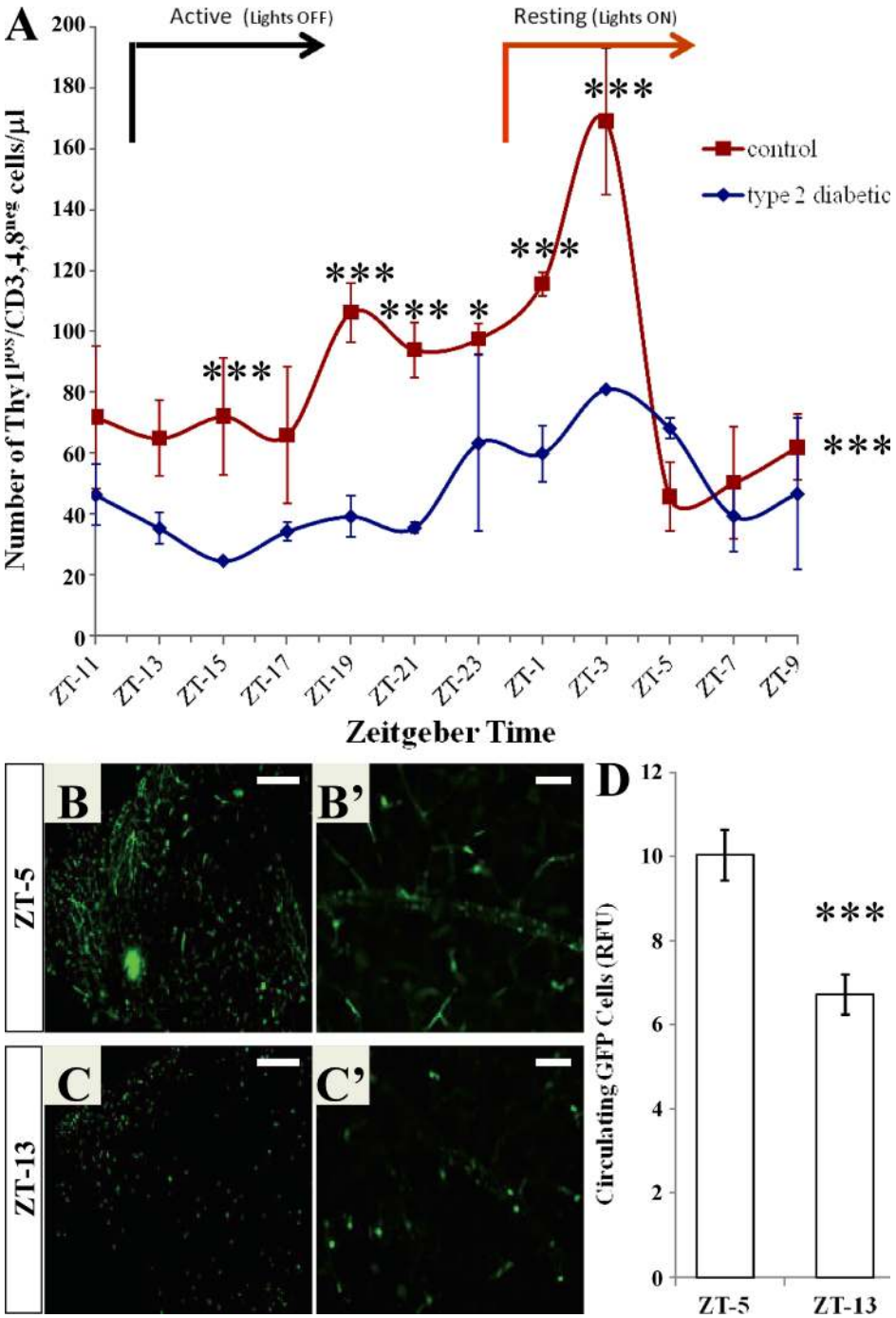

Figure 4. Diabetes decreases circadian release of EPCs. (A) Control (n = 4) and diabetic (n = 3) rats were maintained on a 12/12 h light/dark cycle (lights on at ZT-0, lights off at ZT-12). 100 µl of blood was taken every 2 h and analyzed for the number of EPCs by flow cytometry. EPCs were determined as number of thy-1^{+}CD3^{-}CD4^{-}CD8^{-} cells per µl of blood. There is a clear peak in the EPC number at ZT-3 in control animals (red line). However, the response is blunted in Type 2 (blue line) diabetic animals. The number of EPCs in blood was consistently lower in type 2 diabetic animals compared with control animals. The data represent the mean ± SD. The experiment was performed on two independent sets of animals, with 12 repetitions per animal. Statistical analysis was performed using two-way ANOVA for diabetes and time effect (***, $P < 0.0001$) and Bonferroni post-test to compare replicates by row (*, $P < 0.05$; ***, $P < 0.001$). (B) Circadian variation in the number of bone marrow–derived cells in the retinal circulation of mice. Retinal flat mounts from gfp^{+} chimeric control mice show increased numbers of bone marrow–derived circulating cells (green) in the retinal capillaries at ZT-5 (B and B′) as compared with ZT-13 (C and C′). 10 fields per retina were evaluated and both retinas per mouse were analyzed. Magnification is 4× in B and C and 20× in B′ and C′. Bars: (B and C) 100 µm; (B′ and C′) 10 µm. (D) Quantification of gfp^{+} cells shows an increase in green fluorescence in retinal capillaries at ZT-5 as compared with ZT-13 (n = 4; ***, $P < 0.001$). The data represents mean ± SE. The experiment was performed on three independent sets of animals, with the total number of mice per time point equal to nine.

demonstrated a dramatic drop to baseline EPC numbers immediately after the ZT-3 peak. In contrast, diabetic rats lost this abrupt drop. This finding was confirmed in the type 1 diabetic animal model (Fig. S1 A).

We interpreted the persistent elevation of EPCs until ZT-7 in diabetics as reduced release and also diminished clearance of these cells from the blood. This reduced clearance was likely the result of a diminished ability of EPCs to migrate into tissues from the circulation and is in keeping with the profound migratory defect of these cells observed in diabetes (Segal et al., 2006; Fig. S3).

To further explore this possibility, we generated chimeric mice that underwent transplantation with bone marrow HSCs from gfp homozygous transgenic mice and then were stably engrafted for 4 mo. Retinal flat mounts were prepared from animals euthanized at either ZT-5 (peak of rest phase in mice) or ZT-13 (trough of EPC release in circulation). In agreement with thy-1 enumeration data in healthy rats (Fig. 4 A), many more gfp^+ cells were present in the retinal circulation at the peak release for mice, ZT-5, as compared with ZT-13 (Fig. 4, B–D).

We thus postulated that in diabetes, the EPCs were trapped within the diabetic bone marrow as a result of a lack of sympathetic innervation and reduced NE release. To test this, we examined the bone marrow in the same rats that underwent 24-h blood sampling for EPC enumeration. These diabetic rats with decreased peripheral blood EPCs showed a marked elevation in the number of bone marrow EPCs

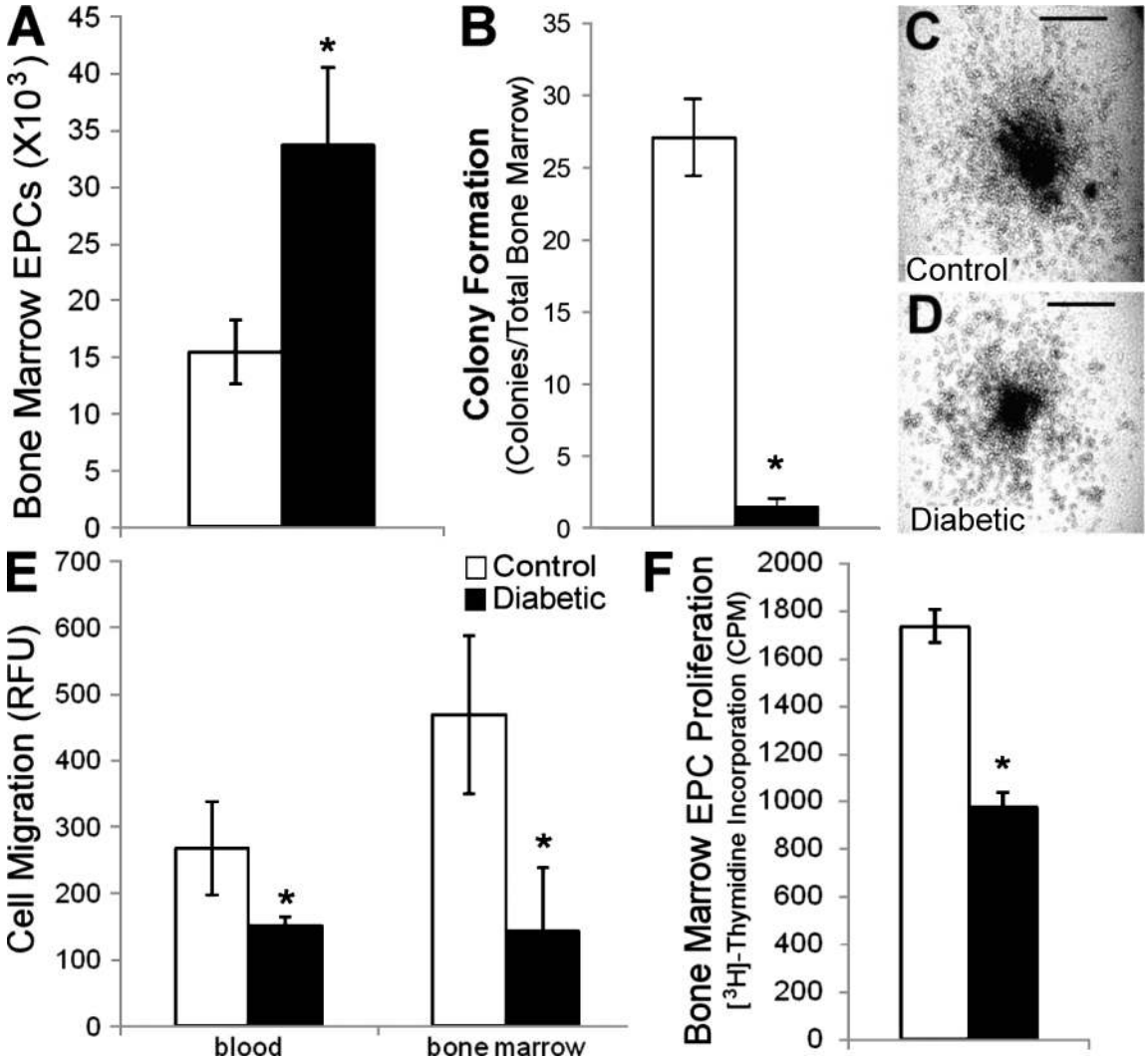

Figure 5. Characterization of thy-1⁺ EPC number and function in type 2 diabetic rats. (A) Diabetic rats ($n = 3$; black) with decreased peripheral blood EPCs showed a marked increase in the number of bone marrow EPCs compared with controls ($n = 6$; white). (B) Diabetic bone marrow (black) showed a reduction in CFU compared with healthy controls (white). (C and D) Typical colony formation observed from explanted control (C) and diabetic EPCs (D). Bars, 100 µM. (E) Both blood and bone marrow EPCs of diabetic origin (black) demonstrate reduced migration to VEGF compared with control (white). (F) Diabetic bone marrow EPCs (black) show reduced proliferation compared with control cells (white). The data represent the mean ± SE of minimum of four separate experiments. *, $P < 0.05$.

compared with controls (Fig. 5 A). In addition, diabetic bone marrow EPCs showed a reduction in colony formation ability (Fig. 5, B–D) and proliferation (Fig. 5 F). Both blood and bone marrow EPCs had a reduced migration to VEGF (Fig. 5 E) compared with age-matched controls.

We reasoned that circulating NE levels in these diabetic animals with peripheral neuropathy and retinopathy may be altered and then measured NE levels in the blood of these rats. Control rats had two distinct peaks of plasma NE levels, one at ZT-1 and one at ZT-13 (Fig. S1 B). Interestingly, in diabetic animals, the first NE peak at ZT-1 was considerably higher and broader than in controls, showing a compensatory adrenal response, whereas the second peak at ZT-13 was absent, supporting the concept of sympathetic dysfunction in these rats.

These experiments demonstrate that type 2 diabetes is associated with a reduction in circadian release of EPCs from the bone marrow. Because circadian rhythm is under tight control of not only the central clock, the SCN, but also peripheral clocks, we next examined whether clock gene expression in the SCN, retina, bone marrow, and peripheral blood EPCs was altered in diabetes. At peak release of EPCs, animals were sacrificed and their SCN brain regions, retinas, bone marrow, and peripheral blood harvested for messenger RNA (mRNA) extraction. Clock genes (*Clock*, *Bmal1*, *Per-1*, *Per-2*, *CRY-1*, *CRY-2*, *ERB*, and *RORA*) were quantified by real-time PCR in these tissues and cells. Rats with diabetes demonstrated a significant decrease ($P < 0.05$) in expression of these clock genes in the retina and in thy-1^+ cells

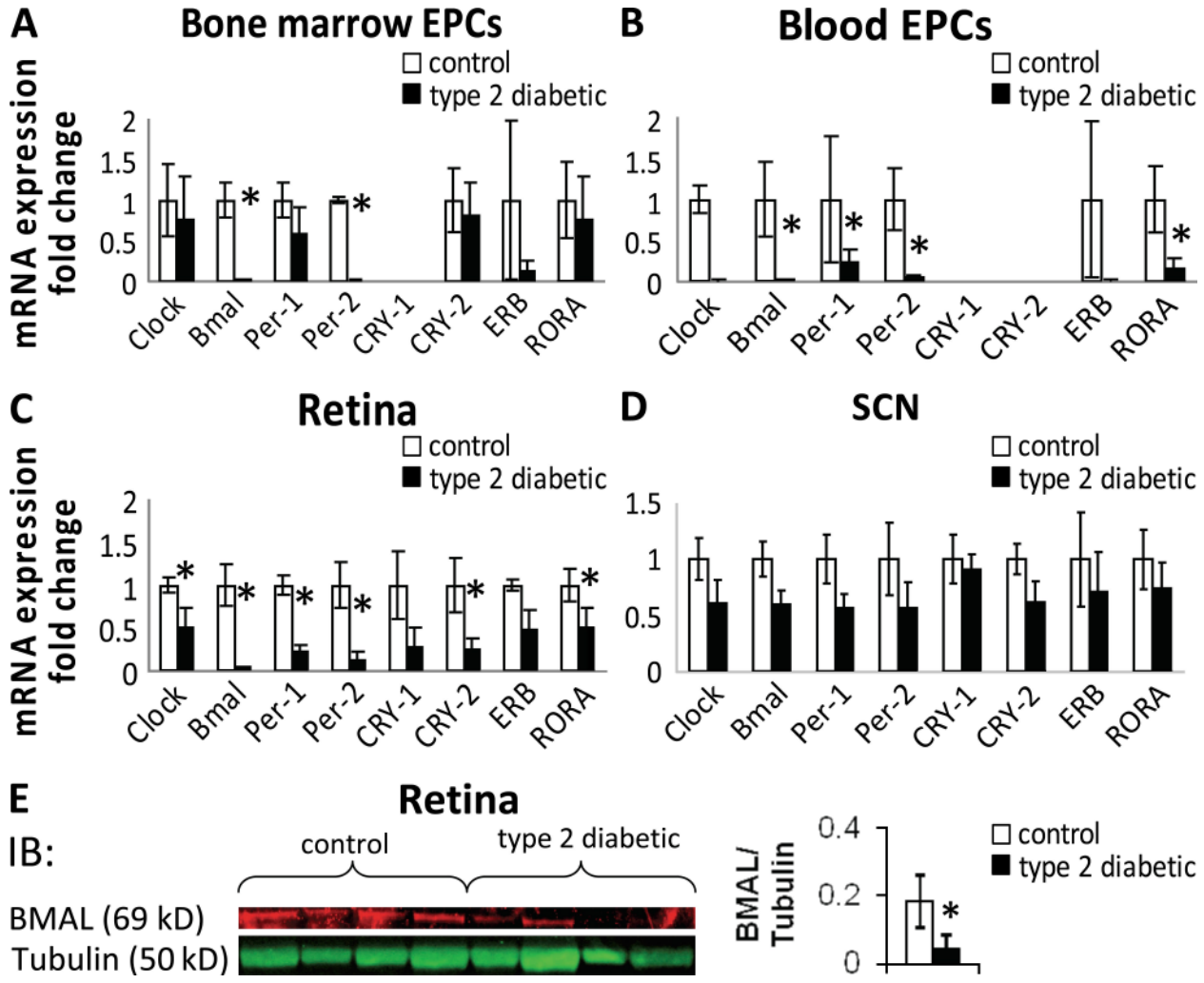

Figure 6. Clock gene expression analysis. Rats used in the circadian rhythm study were sacrificed during the peak time of EPC release, ZT1–5, 24 h after blood collection. (A–D) RNA extracted from total retina (A), peripheral blood thy-1^+ (B), bone marrow thy-1^+ populations (C) and SCN (D) were analyzed for the clock genes *Clock*, *Bmal1*, *Per1*, *Per2*, *CRY1*, *CRY2*, *ERB*, *and RORA*. Clock genes demonstrate reduced expression in the diabetic retinas and thy-1^+ cells. In the bone marrow fraction, Bmal1 and Per2 were significantly reduced in diabetic animals. Although changes in SCN were not significant, means for all clock genes were lower in diabetes. The mRNA expression levels were normalized to cyclophilin and expressed as fold change over control animals. (E) Western blotting from the retina demonstrated reduction of BMAL in diabetes. The quantitative PCR data are presented as the mean ± SE and the Western blotting represents a mean ± SD of four control and three diabetic animals. The experiment was performed on two independent sets of animals with triplicate measurements for quantitative PCR and duplicate Western blots. *, $P < 0.05$ compared with control.

isolated from both blood and bone marrow (Fig. 6, A–C). Protein studies revealed reduction in Bmal expression in diabetic rats as compared with controls (Fig. 6 E). This dramatic reduction in both the positive and negative arms of circadian gene regulators would lead to dampened oscillations and lower and broader peaks, which is the pattern we observed in the circulating EPCs in diabetic rats compared with age-matched controls. Healthy rats, in contrast, demonstrated a higher narrower peak than the diabetic rats. Although expression of clock genes was reduced in the SCN regions of diabetic rats, the difference from controls was not significant (Fig. 6 D). This lack of change suggests that diabetes is associated with dysfunction of the peripheral rather than the central clock. The mRNA and protein expression of clock genes in control and diabetic human retina (Fig. S2) is in agreement with the alterations of clock gene expression found in the diabetic rat model.

The potential to form new blood vessels and repair damaged vessels depends on the EPCs' ability to both leave the bone marrow and to migrate toward the site of angiogenesis. In this study, we observed that type 2 diabetic rats demonstrate the hallmark feature of diabetic retinopathy, acellular capillaries within the retina, at the precise time when there is denervation of the bone marrow and a reduction in peripheral clock gene expression. The resultant acellular capillaries seen at 4 mo of diabetes appear to be caused, in part, by the loss of proper EPC reparative function and by failure of circadian EPC release secondary to diabetes-associated denervation of the bone marrow. In the presence of innervation, as observed in control rats, there was normal retinal histology and a robust circadian release of EPC from the bone marrow. We report that by 4 mo of diabetes in our model of type 2 diabetes, there is inherent sympathetic denervation that can alter circadian release of EPC from the bone marrow. Our data supports that the loss of circadian EPC release results in inadequate levels of cells in the circulation at the optimal time of repair (rest phase) and that this defect, in addition to defects of EPC function (reduced proliferation and migration), contributes to the development of diabetic retinopathy.

Circadian dysfunction itself can have profound effects on the diabetic state. Prior work has shown that mice with a specific clock gene mutation demonstrate impaired endothelial function, including decreased tube formation and faster senescence and impaired EPC-mediated repair (Wang et al., 2008). Other clock genes have been shown to directly regulate glucose homeostasis, and their inactivation suppresses diurnal variation in glucose and triglycerides along with reduced gluconeogenesis (Kohsaka et al., 2007). Our novel findings would indicate that restoration of sympathetic innervation to the diabetic bone marrow should result in physiological EPC egress from the bone marrow and improved retinal vascular repair (Thomas et al., 2008). Moreover, strategies to normalize peripheral clock gene expression may be a novel way to both treat and prevent the development of diabetic macro- and microvascular complications by circumventing sympathetic nervous system dysfunction.

MATERIALS AND METHODS

Femoral arterial catheterization. The protocols for the rat studies were approved by the Institutional Animal Care and Use Committee at Michigan State University, The University of Florida, and Biomedical Research Models, Inc. Multiple blood draws were performed by direct catheter placement into the femoral artery and vein. Animals were anesthetized with isoflurane (2%). The surgical approach for the femoral arterial catheters was through the ventral aspect of the leg. The catheters were tunneled subcutaneously to the nape of the neck and secured with sutures for later access while the animals were conscious. Blood draws were initiated after complete recovery of the animal, as determined by healing of the incision sites, usually 3–4 d after surgery. Blood draws (100 µl each) were performed every 2 h for 24 h using an Automatic Blood Sampler (DiLab).

Isolation of thy-1$^+$ cells from bone marrow. Rats were euthanized by exsanguination after anesthesia. Rat hind limb bones were dislocated and the skin removed. Bones were flushed with ice cold PBS and the cells pelleted. The cells were then treated with ammonium chloride (STEMCELL Technologies Inc.) to remove any contaminating red blood cells and resuspended in PBS (Mediatech, Inc.) containing 2% FBS and 1 mM EDTA. A custom rat negative selection kit (STEMCELL Technologies Inc.) was used to deplete CD4, CD5, CD8a, and OX-43 cells of the rat. The cells were then further enriched for CD90 (thy-1)-positive cells using a positive selection kit (STEMCELL Technologies Inc.) tagged with a CD90/thy-1 antibody (Abcam).

Flow cytometry analysis. A flow cytometer (LSR II; BD) equipped with FACSDiva software (BD) was used for thy-1$^+$CD3$^-$CD4$^-$CD8$^-$ cell enumeration. PerCP-Cy5.5– (eBioscience), FITC-, RPE-, and Alexa Fluor 647–conjugated mouse anti–rat antibodies (AbD Serotec) were used to stain thy-1, CD3, CD4, and CD8 surface markers, respectively, in concentrations according to the manufacturer's instructions. PerCP-Cy5.5, FITC, and RPE were excited at 488 nm and their respective fluorescent emission was detected at 695, 530, and 576 nm. Alexa Fluor 647 was excited at 633 nm and its emission detected at 660 nm. Isotype-negative samples for all antibodies were used to determine the background fluorescence for each fluorochrome. Single-stained samples were used to set color compensation between fluorochromes. A gate was drawn around the white blood cell population in a forward versus side scatter histogram to exclude red blood cells debris.

NE ELISA. A competitive ELISA kit (ALPCO Diagnostics) was used to determine NE levels in 10 µl of rat plasma according to the manufacturer's instructions. In summary, NE was first extracted with a cis-diol–specific affinity gel and then acylated and converted enzymatically. After transfer on antiserum-covered microtiter plates, derivatized samples competed with solid phase–bound analytes for a fixed number of binding sites. After free analytes were removed by washing, the antibody bound to the solid phase was detected by peroxidase conjugation and read at 450 nm. Absorbance reading of the standards (linear) was plotted against known standard concentrations (logarithmic) and a standard curve was drawn to quantify unknown samples.

Immunohistochemistry. Decalcified rat humerus bones were embedded in paraffin, sectioned on a rotary microtome at 4 µm, and then dried and deparaffinized. Enzymatic epitope retrieval was performed. After pretreatments, standard Avidin–Biotin complex staining steps were performed at room temperature on an Autostainer (Dako). After blocking nonspecific protein with nonimmune goat serum (Vector Laboratories), sections were incubated with an Avidin (Vector Laboratories)/Biotin (Sigma-Aldrich) blocking system. Polyclonal rabbit anti-NF200 (Sigma-Aldrich) at 1:100 or polyclonal rabbit anti-TH (Millipore) at 1:100 in normal antibody diluent (ScyTek Laboratories) was used for staining. Biotinylated secondary goat anti–rabbit IgG (Vector Laboratories) in normal antibody diluent diluted 1:400, followed by R.T.U. Elite Peroxidase reagent (Vector Laboratories), was applied for visualization. The slides were developed using Nova red (Vector Laboratories), counterstained using Gill (Lerner) 2 Hematoxylin (Thermo Fisher Scientific), dehydrated, cleared, and mounted using Permount (Thermo Fisher Scientific).

Retinal vasculature preparation. The sensory retina was isolated by gently separating it from pigment epithelium and choroid using a #00 paint brush under a dissecting microscope, prepared using trypsin digestion, and stained with hematoxylin and periodic acid–Schiff (Mizutani et al., 1996). Acellular capillaries were quantified in a masked manner by three independent examiners.

gfp bone marrow chimeric mice. 10–12-wk-old female C57BL6/J mice were lethally irradiated and then their bone marrow was reconstituted with lineage-negative $Sca1^+$ $c\text{-}kit^+$ HSCs from donor bone marrow of transgenic mice homozygous for gfp, according to methods published previously (Grant et al., 2002). At selected times (ZT-5 And ZT-13) mice were euthanized and blood was collected for enumeration of thy-1^+gfp^+ circulating cells. The eyes were enucleated and preserved, retinas dissected, and mounted flat and image captures made using a fluorescent microscope (Eclipse TE200; Nikon) equipped with a digital camera (SPOT0.60XHRD06-NIK; Diagnostic Instruments, Inc.).

Real-time quantitative RT-PCR. Rat retinas and bone marrow or blood EPCs were homogenized in Trizol reagent (Invitrogen), and RNA was isolated according to the manufacturer's instructions. First-strand complementary DNA was synthesized from isolated RNA using SuperScript II reverse transcription (Invitrogen). Prepared complementary DNA was mixed with 2× SYBR Green PCR Master Mix (Applied Biosystems) and various sets of gene-specific (Table S1) forward and reverse primers and subjected to real-time PCR quantification using the ABI PRISM 7700 Sequence Detection System (Applied Biosystems). All reactions were performed in triplicate. The relative amounts of mRNAs were calculated using the comparative threshold cycle method. Cyclophilin was used as a control, and all results were normalized to the abundance of cyclophilin.

Thymidine proliferation assay. 30,000 EPCs were plated per well using a 24-well plate and then treated with cytokine mix (Stem Cell Technologies) for 12 h. Thymidine was diluted 1:10 in PBS and added to the wells directly. The cells were then placed in the CO_2 incubator for 2 h. Then cells were removed, spun at 5,000 rpm for 5 min, and washed with ice cold 10% TCA (×2). 0.2 M NaOH was added to the cells and the plates were shaken gently for 10 min at room temperature. 100 µl of cell homogenate was then added to 4 ml Cytoscint (Thermo Fisher Scientific). CPM was counted using thymidine settings.

Online supplemental material. Fig. S1 depicts decreased number of circulating EPCs in a type 1 diabetes model, increased plasma levels of NE in a type 2 diabetes model, and decreased number of circulating CD3-positive cells in a type 2 model as compared with controls. In Fig. S2, we show that clock genes demonstrate altered mRNA and protein levels in human diabetic retina. Fig. S3 illustrates that normal, but not diabetic, human EPC may participate in ocular vascular reendothelialization in diabetic mice. Table S1 shows real-time RT-PCR primers. Online supplemental material is available at http://www.jem.org/cgi/content/full/jem.20090889/DC1.

The authors thank Carrie Northcott, J.R. Haywood, Hannah Garver, Gregory Fink, and Sachin Kandlikar for training and assistance with femoral artery catheterization surgery and Tara Galvin and Jared Rice for providing the DiLab automated blood sampler and helping with the initial setup and data collection. Technical support was provided by Amy S. Porter, Kathleen A. Joseph, Ricky A. Rosebury, Svetlana Bozack, and Lily Yan from the Michigan State University and Sugata Hazra from the University of Florida.

This work was supported by grants from the National Institutes of Health (EY007739 and EY012601 to M.B. Grant and EY016077 to J.V. Busik), Juvenile Diabetes Research Foundation (4-2000-847 to M.B. Grant and 2-20005-97 to J.V. Busik), American Heart Association (M.B. Grant), and Michigan Agricultural Experimental Station (MICL02163 to J.V. Busik).

The authors have no conflicting financial interests.

Submitted: 22 April 2009
Accepted: 28 October 2009

REFERENCES

Asahara, T., T. Murohara, A. Sullivan, M. Silver, R. van der Zee, T. Li, B. Witzenbichler, G. Schatteman, and J.M. Isner. 1997. Isolation of putative progenitor endothelial cells for angiogenesis. *Science*. 275:964–967. doi:10.1126/science.275.5302.964

Ellis, E.A., M.B. Grant, F.T. Murray, M.B. Wachowski, D.L. Guberski, P.S. Kubilis, and G.A. Lutty. 1998. Increased NADH oxidase activity in the retina of the BBZ/Wor diabetic rat. *Free Radic. Biol. Med*. 24:111–120. doi:10.1016/S0891-5849(97)00202-5

Ellis, E.A., D.L. Guberski, M. Somogyi-Mann, and M.B. Grant. 2000. Increased H2O2, vascular endothelial growth factor and receptors in the retina of the BBZ/Wor diabetic rat. *Free Radic. Biol. Med*. 28:91–101. doi:10.1016/S0891-5849(99)00216-6

Grant, M.B., W.S. May, S. Caballero, G.A. Brown, S.M. Guthrie, R.N. Mames, B.J. Byrne, T. Vaught, P.E. Spoerri, A.B. Peck, and E.W. Scott. 2002. Adult hematopoietic stem cells provide functional hemangioblast activity during retinal neovascularization. *Nat. Med*. 8:607–612. doi:10.1038/nm0602-607

Ikeda, H., Q. Yong, T. Kurose, T. Todo, W. Mizunoya, T. Fushiki, Y. Seino, and Y. Yamada. 2007. Clock gene defect disrupts light-dependency of autonomic nerve activity. *Biochem. Biophys. Res. Commun*. 364:457–463. doi:10.1016/j.bbrc.2007.10.058

Katayama, Y., M. Battista, W.M. Kao, A. Hidalgo, A.J. Peired, S.A. Thomas, and P.S. Frenette. 2006. Signals from the sympathetic nervous system regulate hematopoietic stem cell egress from bone marrow. *Cell*. 124:407–421. doi:10.1016/j.cell.2005.10.041

Kohsaka, A., A.D. Laposky, K.M. Ramsey, C. Estrada, C. Joshu, Y. Kobayashi, F.W. Turek, and J. Bass. 2007. High-fat diet disrupts behavioral and molecular circadian rhythms in mice. *Cell Metab*. 6:414–421. doi:10.1016/j.cmet.2007.09.006

Loomans, C.J., H. Wan, R. de Crom, R. van Haperen, H.C. de Boer, P.J. Leenen, H.A. Drexhage, T.J. Rabelink, A.J. van Zonneveld, and F.J. Staal. 2006. Angiogenic murine endothelial progenitor cells are derived from a myeloid bone marrow fraction and can be identified by endothelial NO synthase expression. *Arterioscler. Thromb. Vasc. Biol*. 26:1760–1767. doi:10.1161/01.ATV.0000229243.49320.c9

Méndez-Ferrer, S., D. Lucas, M. Battista, and P.S. Frenette. 2008. Haematopoietic stem cell release is regulated by circadian oscillations. *Nature*. 452:442–447. doi:10.1038/nature06685

Mizutani, M., T.S. Kern, and M. Lorenzi. 1996. Accelerated death of retinal microvascular cells in human and experimental diabetic retinopathy. *J. Clin. Invest*. 97:2883–2890. doi:10.1172/JCI118746

Peichev, M., A.J. Naiyer, D. Pereira, Z. Zhu, W.J. Lane, M. Williams, M.C. Oz, D.J. Hicklin, L. Witte, M.A. Moore, and S. Rafii. 2000. Expression of VEGFR-2 and AC133 by circulating human CD34(+) cells identifies a population of functional endothelial precursors. *Blood*. 95:952–958.

Peschke, E. 2008. Melatonin, endocrine pancreas and diabetes. *J. Pineal Res*. 44:26–40.

Ruiter, M., R.M. Buijs, and A. Kalsbeek. 2006. Hormones and the autonomic nervous system are involved in suprachiasmatic nucleus modulation of glucose homeostasis. *Curr. Diabetes Rev*. 2:213–226. doi:10.2174/157339906776818596

Said, G. 2007. Focal and multifocal diabetic neuropathies. *Arq. Neuropsiquiatr*. 65:1272–1278.

Schatteman, G.C., M. Dunnwald, and C. Jiao. 2007. Biology of bone marrow-derived endothelial cell precursors. *Am. J. Physiol. Heart Circ. Physiol*. 292:H1–H18. doi:10.1152/ajpheart.00662.2006

Segal, M.S., R. Shah, A. Afzal, C.M. Perrault, K. Chang, A. Schuler, E. Beem, L.C. Shaw, S. Li Calzi, J.K. Harrison, et al. 2006. Nitric oxide cytoskeletal-induced alterations reverse the endothelial progenitor cell migratory defect associated with diabetes. *Diabetes*. 55:102–109. doi:10.2337/diabetes.55.01.06.db05-0803

Serre, C.M., D. Farlay, P.D. Delmas, and C. Chenu. 1999. Evidence for a dense and intimate innervation of the bone tissue, including glutamate-containing fibers. *Bone*. 25:623–629. doi:10.1016/S8756-3282(99)00215-X

Su, W., Z. Guo, D.C. Randall, L. Cassis, D.R. Brown, and M.C. Gong. 2008. Hypertension and disrupted blood pressure circadian rhythm in type 2

diabetic db/db mice. *Am. J. Physiol. Heart Circ. Physiol.* 295:H1634–H1641. doi:10.1152/ajpheart.00257.2008

Thomas, H.E., R. Redgrave, M.S. Cunnington, P. Avery, B.D. Keavney, and H.M. Arthur. 2008. Circulating endothelial progenitor cells exhibit diurnal variation. *Arterioscler. Thromb. Vasc. Biol.* 28:e21–e22. doi:10.1161/ATVBAHA.107.160317

Tirabassi, R.S., J.F. Flanagan, T. Wu, E.H. Kislauskis, P.J. Birckbichler, and D.L. Guberski. 2004. The BBZDR/Wor rat model for investigating the complications of type 2 diabetes mellitus. *ILAR J.* 45:292–302.

Wang, C.Y., M.S. Wen, H.W. Wang, I.C. Hsieh, Y. Li, P.Y. Liu, F.C. Lin, and J.K. Liao. 2008. Increased vascular senescence and impaired endothelial progenitor cell function mediated by mutation of circadian gene Per2. *Circulation.* 118:2166–2173. doi:10.1161/CIRCULATIONAHA.108.790469

Weber, F. 2009. Remodeling the clock: coactivators and signal transduction in the circadian clockworks. *Naturwissenschaften.* 96:321–337. doi:10.1007/s00114-008-0474-9

Weston, P.J., and G.V. Gill. 1999. Is undetected autonomic dysfunction responsible for sudden death in Type 1 diabetes mellitus? The 'dead in bed' syndrome revisited. *Diabet. Med.* 16:626–631. doi:10.1046/j.1464-5491.1999.00121.x